
Article:
Schofield, L., Smith, L., Marshall, H. et al. (2026) Structure and function imaging in primary ciliary dyskinesia: cross-sectional study with 129Xe ventilation / 1H anatomical MRI. ERJ Open Research. 00984-2025. ISSN: 2312-0541

https://doi.org/10.1183/23120541.00984-2025

ERJ open research
THE BEST IN OPEN ACCESS BASIC, TRANSLATIONAL & CLINICAL RESPIRATORY RESEARCH

Early View

Original Research Article

Structure and function imaging in Primary ciliary dyskinesia: cross-sectional study with ^{129}Xe ventilation / ^{1}H anatomical MRI

Lynne Schofield, Laurie Smith, Helen Marshall, David Hughes, Alberto Biancardi, Jody Bray, Dave Capener, Guilheim Collier, Shahgufta Fazal, Eduardo Moya, Ryan Munro, Graham Norquay, Evie Robson, Oliver Rodgers, Susanne Shanks, Anna Shawcross, Sally J Singh, Neil Stewart, Noreen West, Anna Zalewska, Daniel Hind, Jim M Wild

Please cite this article as: Schofield L, Smith L, Marshall H, *et al*. Structure and function imaging in Primary ciliary dyskinesia: cross-sectional study with ^{129}Xe ventilation / ^{1}H anatomical MRI. *ERJ Open Res* 2026; in press (https://doi.org/10.1183/23120541.00984-2025).

ERJ Open Research

Structure and function imaging in Primary ciliary dyskinesia: cross-sectional study with ^{129}Xe ventilation / ^{1}H anatomical MRI

Lynne Schofield[1,2,3], Laurie Smith[1], Helen Marshall[1,10], David Hughes[4], Alberto Biancardi[1,10], Jody Bray[1], Dave Capener[1], Guilheim Collier[1,10], Shahgufta Fazal[1], Eduardo Moya[5], Ryan Munro[1] , Graham Norquay[1], Evie Robson[2], Oliver Rodgers[1], Susanne Shanks[6], Anna Shawcross[7], Sally J Singh[8], Neil Stewart[1,10], Noreen West[4], Anna Zalewska[1] , Daniel Hind[9], Jim M Wild[1,10].

Affiliations

1. POLARIS, School of Medicine and Population Health, University of Sheffield.
2. Leeds Children's Hospital at Leeds Teaching Hospitals.
3. Child Health Outcomes Research at Leeds (CHORAL), University of Leeds, Leeds. www.choralresearch.org.uk
4. Sheffield Children's Hospital, Sheffield, UK.
5. Bradford Teaching Hospitals, Bradford, UK.
6. Patient parent representative.
7. Royal Manchester Children's Hospital, Manchester, UK.
8. Department of Health Sciences, University of Leicester, Leicester, UK.
9. School of Healthcare, University of Leeds, Leeds, UK.
10. Insigneo Institute, University of Sheffield.

Corresponding author:

Lynne Schofield
lynneschofield@nhs.net
Paediatric physiotherapy, Leeds Teaching Hospitals
North Wing 2nd floor, 2 Park Lane, Leeds, LS3 1ES.

Summary

Most clinically stable children with PCD had visible ventilation abnormalities when assessed with ^{129}Xe MRI. ^{129}Xe derived VDP was abnormal in 75% of children who had a normal FEV_1.

Abstract

Background

In Primary ciliary dyskinesia (PCD), impaired mucociliary clearance leads to respiratory infections. Whilst FEV_1 is commonly used to evaluate lung function in PCD its sensitivity to detect abnormalities in mild disease is limited. This study explores the utility of ^{129}Xe ventilation and ^{1}H anatomical magnetic resonance imaging (MRI) to assess lung health in children with PCD.

Methodology

This prospective cohort study assessed clinically stable children with PCD (aged 5-18 years) using ^{129}Xe MRI, ^{1}H MRI and spirometry during one session. Ventilation defect percentage (VDP) was the primary metric calculated from ^{129}Xe MRI.

Results

35 children were assessed, mean age= 12.3 ± 3.3 years, FEV_1 z-score= -1.5 ± 1.7. Most children had visible ventilation abnormalities and 82.8% had an abnormal ^{129}Xe VDP, median (IQR) ^{129}Xe VDP=6.3 (1.3,16.1)%. 16 participants had a normal FEV_1 (z-score > -1.6), however 12 of these individuals had abnormal ^{129}Xe VDP. ^{1}H MRI found 55.9% participants had a region of collapse; 58.1% had bronchiectasis; and 50.0% had evidence of air trapping.

Conclusion

^{129}Xe MRI can identify early lung function abnormalities in children with PCD and demonstrates that the extent of ventilation distribution abnormalities in PCD varies between individuals. ^{1}H MRI provides complementary diagnostic information on structural abnormalities.

Introduction

Primary ciliary dyskinesia (PCD) is an inherited condition in which structural and/or functional cilial abnormalities impair mucociliary clearance. People with PCD (PwPCD) experience chronic infections with exacerbations of the upper and lower respiratory tract, fueling inflammation and the development of bronchiectasis (1). Whilst forced expiratory volume in the first second (FEV_1) from spirometry is the most widely used clinical outcome measure in PCD, large variability in FEV_1 is seen during periods of disease stability (2). Additionally, FEV_1 can be insensitive to detect abnormalities; 73% of PwPCD with structural lung abnormalities on computerised tomography (CT) scan have an FEV_1 within the normal range (3). Whilst lung clearance index (LCI) from multiple breath washout is more sensitive to detect lung abnormalities than FEV_1 (4), the correlation of LCI with other outcomes remains unclear (5). As such, more sensitive outcome measures are needed to accurately assess lung abnormalities in PCD.

Hyperpolarised gas ventilation magnetic resonance imaging (MRI) using helium-3 (^3He) or xenon-129 (^{129}Xe) (6) permits the visualisation and quantitative assessment of the distribution of ventilation within the lung in 3-dimensions. ^{129}Xe which is more readily available than ^3He is now commonly used in hyperpolarised gas MRI research (6) and offers potential clinical application (7). Ventilation abnormalities, visible as areas without gas signal, are known as ventilation defects. Ventilation defect percentage (VDP), the proportion of the thoracic cavity with no gas signal, is the most commonly used metric. Hyperpolarised gas ventilation MRI has shown promise in evaluating lung ventilation defects in other chronic suppurative lung diseases (CSLDs) (8), but its application in PCD to date has been limited. VDP is a sensitive marker of lung health in cystic fibrosis (CF) (8-10) and other obstructive lung diseases (6). In a small study of children with PCD, ^3He VDP was found to be more sensitive to detect abnormalities than LCI and FEV_1 (11), however there are no published data using ^{129}Xe MRI to assess PwPCD. Recognising that it is a safe, ionising radiation-free, and well tolerated technique (6), children with PCD and parent representatives were supportive of research to explore the utility of ^{129}Xe MRI.

^{1}H MRI of the lungs can identify structural abnormalities without ionising radiation and does not require access to hyperpolarised gas technology. Findings from ^{1}H Ultrashort echo-time (UTE) MRI sequences are increasingly comparable with CT imaging findings, and offer longitudinal assessment capability in CSLDs (12). In some centres ^{1}H MRI is used for routine clinical assessment of people with CF (13). In PCD, ^{1}H MRI can identify collapse, consolidation, mucus plugging and bronchiectasis (14) and agreement has been seen between abnormalities identified on ^{1}H MRI and high-resolution computerised tomography (HRCT) (15). Functional abnormalities have been identified in PwPCD previously using the Matrix pencil ^{1}H MRI (MP-MRI) method, but this had lower spatial resolution and was less sensitive than UTE structural MRI to detect abnormalities (3).

This study aimed to assess lung physiology and structure in children and young people with PCD using ^{129}Xe ventilation and ^{1}H anatomical MRI. This work is part of a larger study (16) which assessed lung health with ^{129}Xe MRI on the same day before and after airway clearance, this paper summarises the cross-sectional data from the study population.

Methods

This prospective study recruited children (aged 5 to 18 years) with PCD from four centres in the North of England between April 2022 and August 2023. For inclusion, participants needed to: have a confirmed PCD diagnosis according to the ERS guidelines (17), be clinically stable at the time of the assessment (not on treatment antibiotics for a chest exacerbation), have resting oxygen saturation >90% on air and not have any contraindications to MRI scanning. All eligible participants or their parents/guardians if under 16 years old were approached to take part by members of their direct clinical care team and provided written informed consent. The study was approved by the Oxford B Research ethics committee (21/SC/0197).

Lung imaging

Hyperpolarised ^{129}Xe MRI scanning was performed at a single site (University of Sheffield) on either a 1.5T GE HDxt, or 1.5T GE Artist MRI scanner (GE, Milwaukee, WI, USA) using a ^{129}Xe transmit-receive vest coil (Clinical MR Solutions, Brookfield,

WI, USA). ^{129}Xe MR images were acquired using a 3D steady state free precession (SSFP) sequence (18). The ^{129}Xe gas was polarised using an in-house polariser under regulatory licence (MS-18739) (19). Images were acquired during a breath-hold at an end-inspiratory tidal volume (EITV), following inhalation of a titrated mixture of ^{129}Xe and medical grade Nitrogen, administered via a Tedlar plastic bag from residual volume. The total volume of inhaled gas was calculated based on participant's height and ranged between 0.4 and 1.0 Litre (20). To estimate the thoracic cavity for image analysis, ^{1}H 3D spoiled gradient echo (SPGR) MR images were acquired pre and post the ^{129}Xe images during separate matched breath-holds at EITV. ^{129}Xe images were segmented using a semi-automated method (21) to calculate ^{129}Xe VDP and the ventilation heterogeneity index (VHI) (22) was also assessed.

^{1}H imaging sequences included:

- 3D SPGR acquired at two lung inflation levels: functional residual capacity plus inhaled bag volume (i.e. EITV), and residual volume (RV),
- Radial 3D UTE during free breathing (23),
- 2D SSFP at expiratory breath-hold,
- 2D T2-weighted Half-Fourier Acquisition Single-shot Turbo spin Echo imaging (HASTE) at expiratory breath-hold).

These were performed using an 8-channel or 16+ channel anterior array plus a spine ^{1}H array (HDxt and Artist MRI scanner respectively) (GE, Milwaukee, WI, USA) to provide high resolution anatomical images. A consultant paediatric radiologist reviewed all images to assess for typical PCD features including bronchiectasis, collapse, consolidation, and air trapping. Participants were imaged at three times on the same day (see OLS for study schedule). Baseline ^{1}H imaging was primarily used to assess for abnormalities, however where baseline images were not readable, ^{1}H MR images from later time points were used.

Further details on sequence details, image acquisition, processing, and calculation of ^{129}Xe MRI metrics are provided in the supplementary information.

Acquisition of non-imaging data

Clinical and diagnostic information were obtained prior to the study visit from medical notes and the clinical team. Spirometry was performed immediately prior to the first MRI scan with a 'PFT Pro' (Vyaire, Basingstoke, UK) in accordance with technical standards (24). All spirometry metrics were assessed using a z-score, with -1.64 used as the lower limit of normal (25). Quality of life was assessed on the same day using the age-appropriate version of the QOL-PCD online questionnaire: adolescent for aged 13-17 years and child and parent proxy for those aged under 13 years (26).

Statistical analysis

Statistical analysis was performed using GraphPad (Prism version 9.5.1, San Diego, US). Normal distribution was assessed using the Shapiro–Wilk test. Data are presented as mean ± SD, if they are normally distributed, or median (range) otherwise. Group comparisons were completed using the un-paired t-test, Mann-Whitney U test (not normal distribution), parametric analysis of variance test or Kruskal-Wallis analysis of variance test, depending on data distribution and number of groups. Correlation was assessed using Spearman's rank-based correlation. Statistical significance was defined as $p<0.05$. ^{129}Xe VDP of 1.2% and VHI of 9.5% were used as the upper limits of normal from a population of children without history of lung disease (27).

Results

93 individuals were assessed for eligibility; 15 did not meet inclusion criteria and 76 were approached. 36 individuals consented to participate of which 35 young people were assessed with ^{129}Xe and ^{1}H MRI and one individual withdrew due to intolerance of the scanner sounds. 35 participants were assessed with QOL-PCD in total: adolescent version (n=16), both child and parent-proxy versions (n=14), child version (n=3), parent-proxy version (n=2). Full details of screening and recruitment are provided in Figure 1. Baseline clinical demographics are provided in Table 1 and QOL-PCD data in the online supplementary material.

Spirometry

34 individuals performed technically acceptable spirometry (28) (Table 2), one data set was not technically acceptable and was excluded. 55.8% (n=19) had no evidence of airway obstruction (FEV_1/FVC z-score >-1.64). No correlation was seen between FEV_1 and age, age at diagnosis, number of antibiotic courses or lower respiratory symptoms/physical functioning QOL-PCD domains. No significant differences in FEV_1 were seen between ultrastructural defect groups, or those who had/had not recently grown Pseudomonas aeruginosa.

^{129}Xe MRI

A summary of ^{129}Xe derived metrics is provided in Table 2 and an image from each of the participants in Figure 2. Most children had visible ventilation abnormalities and 82.8% (n=29) had an abnormal VDP. Six children had very minimal ventilation abnormalities and were comparable to healthy children.

No difference in ^{129}Xe VDP was seen according to sex, or situs abnormalities. No correlation was seen between ^{129}Xe VDP and age, or age at diagnosis. ^{129}Xe VDP was highest in the inner dynein arm (IDA) defects or microtubular disorganisation (MTD) group, with a median (IQR) of 12.8% (1.5, 19.3%). The median (IQR) for the other groups were outer dynein arm defect (ODA), 5.8% (1.8, 7.1%); combined ODA and IDA defects, 9.2% (5.0, 19.6%); and normal ultrastructure with a genetic diagnosis of PCD, 0.4% (0.3, 2.5%). There was no statistically significant difference in ^{129}Xe VDP between the groups.

^{129}Xe VDP correlated moderately with FEV_1 (r=-0.54, p=0.001), FVC (r=-0.42, p=0.01) and FEV1/FVC (r=-0.57, p<0.001) (Figure 3A-C). The number of individuals with abnormal ventilation was greater as assessed by ^{129}Xe VDP when compared to FEV_1; 16 participants had an FEV_1 within the normal range (z-score >-1.64) yet 12 of these individuals (75%) had raised VDP when compared to healthy children (^{129}Xe VDP>1.2%). Two children had a normal VDP (<2.0%) with abnormal spirometry: one with an obstructive pattern (FEV_1/FVC z-score <-1.64 and FEV_1<-1.64) and one with a mixed pattern (FEV_1/FVC z-score <-1.64 and FVC <-1.64). Three children had no evidence of obstruction (FEV_1/FVC z-score >-1.64) but had a restrictive pattern on spirometry (FEV_1 and FVC z-score <-1.64). All of these children had an abnormal VDP (11.0, 11.3 and 27.7%).
Examples of cases in which only one of the two lung health measures were abnormal (either FEV_1 or ^{129}Xe VDP) are shown in Figure 4.

There was no correlation between ^{129}Xe VDP and the number of antibiotics administered in the last 12 months. Whilst ^{129}Xe VDP was higher in individuals who had cultured Pseudomonas aeruginosa (PsA) in the previous 12 months (11.0%) than those who had not (5.4%), this was not statistically significant (p=0.15). Across the three versions of the QOL-PCD, only the social function domain (adolescent version) showed a moderate correlation with ^{129}Xe VDP (r=-0.57, p=0.02).

25 participants (71.4%) had abnormally high ^{129}Xe VHI. ^{129}Xe VHI correlated moderately with spirometry: FEV_1 z-score (r=-0.52, p=0.002); FVC z-score (r=-0.38, p=0.03), and FEV_1/FVC z-score (r=-0.58, p<0.001) (Figure 3D-F). No correlation was seen between ^{129}Xe VHI and age, age at diagnosis, number of antibiotic courses, and lower respiratory/physical functioning QOL-PCD domains. No significant differences in ^{129}Xe VHI were seen between ultrastructural defect groups, or those who had or had not recently grown PsA.

^{1}H MRI assessment of lung structure

Baseline UTE scans were deemed readable for 24/34 (70.1%) participants, a further five participants (14.7%) had unreadable baseline UTE images, but scans from later timepoints within the day were readable. In the remaining five cases image acquisition issues permitted assessment for collapse but not bronchiectasis (n=3). Of those with readable images: 19/31 (61.3%) had bronchiectasis; 19/34 (55.9%) had a region of collapse; 17/34 (50.0%) participants had evidence of air trapping. All 19 with collapse identified had a region of collapse in their middle lobe (right middle lobe in situs solitus and left middle lobe in situs inversus). ^{129}Xe imaging was more sensitive to detect abnormalities than ^{1}H MRI; 4/6 (66.7%) of those with no structural abnormalities had both abnormal VDP and VHI (Figure 5). Figure 6 provides an example visual comparison of abnormalities identified on ^{1}H and ^{129}Xe MRI.

Discussion

This cross-sectional study found that ^{129}Xe MRI detects ventilation abnormalities in most children with PCD. 82.8% of the study population had abnormal ventilation assessed by ^{129}Xe VDP; 75% of individuals with no evidence of obstructive airways disease using spirometry had abnormal ventilation (VDP>1.2%). Whilst ventilation abnormalities were common, a small number of individuals with PCD did not have ventilation abnormalities. ^{1}H MRI also identified structural abnormalities:55.9% of children with PCD had areas of collapse and 61.3% had bronchiectasis.

Our findings are consistent with the previous small study by Smith, West (11) which found VDP (using ^{3}He MRI) to be abnormal in children with PCD who had normal $FEV_{1.}$ With the finding that ^{129}Xe VDP is often abnormal in individuals with a normal FEV_1, our results align with previous hyperpolarised gas MRI literature in CSLDs (9, 11, 20, 29-32). For the first time this study found a small number of children with PCD with abnormal $FEV_{1,}$ including one without restrictive lung disease, but normal ventilation on ^{129}Xe MRI (27). Whilst this study found a moderate correlation of ^{129}Xe VDP with FEV_1 in children with PCD, other studies have reported no corelation between ^{129}Xe VDP with FEV_1 (29), and a stronger correlation between ^{3}He VDP and FEV_1/FVC (11). In paediatric CF, the relationship between ^{129}Xe VDP and FEV_1, is also variable (30, 33, 34). This variability in correlation between VDP and FEV_1 may arise from the differing study populations', or image acquisition methods. These findings illustrate that reliance on spirometry alone for the clinical assessment of lung health in CSLDs may lead to instances of false assurance of normal lung heath. These studies show the importance of using a range of tools to assess different components of lung function in CSLDs.

The clinical picture in PCD is complex; neither spirometry nor ^{129}Xe metrics (VDP and VHI) correlated with age, age at diagnosis, or number of antibiotic courses in the last 12 months, and limited correlation was seen with quality of life assessed by the QOL-PCD. VDP was higher, and FEV_1 lower in those with IDA and ODA defects than those with normal cilial ultrastructure. Previous research reported that individuals with IDA and MTD cilial defects have the highest CT scan disease scores (35), and this study provides further evidence that cilial ultrastructural defects may influence disease severity.

Bronchiectasis, bronchial wall thickening, mucus plugging, and atelectasis are common CT findings in people with PCD (36, 37). The frequency of abnormalities identified in children with PCD using ^{1}H MRI in this study is lower than previously reported: 100% structural abnormalities, 97% and 94% bronchiectasis or wall thickening (3, 14). It is unclear if the lower frequency seen may arise from differences in diagnostic inclusion criteria, image acquisition or a true variance. Finding the anatomical middle lobe, whether located on the left or right side of the body to be a common area of collapse in PCD, this study adds further evidence to the CT scan findings of middle lobe collapse reported by Jain, Padley (38) and highlights the importance of monitoring this area in children with PCD. These data also highlight the potential of ^{1}H MRI to reduce the number of CT scans of the lungs and provides a viable longitudinal lung imaging assessment method.

This is the largest cohort of children with PCD assessed by ^{129}Xe MRI to date, employing a prospective study design with standardised imaging and spirometry methods, an age-appropriate, validated QOL-PCD instrument and clinical data. This study used ^{129}Xe ventilation MRI, a highly sensitive technique, to provide quantitative and qualitative information on the range of functional abnormalities seen in PCD, and ^{1}H anatomical MRI to detect structural abnormalities. Although two children struggled with the MRI scanner noise, one of whom withdrew from the study, the scans were well tolerated by the vast majority of individuals, including those as young as 6 years old. As MRI is ionising radiation-free, it is well placed for assessing children and young people, especially longitudinally. The cross-sectional design precluded assessment of longitudinal changes or inferring causality. Future long-term follow-up studies to determine whether baseline ^{129}Xe VDP predicts key clinical outcomes including exacerbation frequency and lung function decline are needed. Further evaluation of healthy children with ^{129}Xe MRI will provide more robust paediatric reference values enabling multicentre research and clinical implementation of the findings. Whilst high-resolution CT (HRCT) scans were not included to ensure an ionising radiation-free protocol, studies permitting direct comparison of HRCT and ^{1}H MRI in children with CSLDs are warranted. As LCI is widely available, inclusion of LCI in the study protocol would have provided a valuable comparison of ^{129}Xe MRI with LCI. Future work from the ASPECT-PCD study (16) will evaluate the effects of airway clearance techniques using ^{129}Xe MRI.

Conclusion

^{129}Xe ventilation MRI can detect ventilation abnormalities in children with PCD, we also demonstrate that the extent of ventilation distribution abnormalities in PCD varies between individuals. Ventilation abnormalities are identifiable using ^{129}Xe ventilation MRI is children with PCD who have a normal FEV_1. ^{1}H MRI provides complementary diagnostic information on structural abnormalities. ^{129}Xe ventilation MRI offers a sensitive, safe, and well-tolerated imaging technique that is well placed for future longitudinal studies in children with PCD.

Funding

This study was funded by the National institute of health and care research (NIHR301558) and the MRC (MR/M008894/1). This research was supported by Child Health Outcomes Research at Leeds (CHORAL) www.choralresearch.org.uk. CHORAL is funded by Leeds Hospitals Charity, the University of Leeds and Leeds Teaching Hospitals NHS Trust.

References

1. Flume PA, Chalmers JD, Olivier KN. Advances in bronchiectasis: endotyping, genetics, microbiome, and disease heterogeneity. The Lancet. 2018;392(10150):880-90.
2. Rubbo B, Zhang K, Kant A, Borelli M, Constant C, Castillo-Corullón S, et al. Variability of lung function in patients with primary ciliary dyskinesia (PCD): longitudinal analysis from the PROVALF-PCD cohort, a BEAT-PCD Collaboration. European Respiratory Journal 2023 62: PA2760. 2023;62.
3. Nyilas S, Bauman G, Pusterla O, Sommer G, Singer F, Stranzinger E, et al. Structural and Functional Lung Impairment in Primary Ciliary Dyskinesia. Assessment with Magnetic Resonance Imaging and Multiple Breath Washout in Comparison to Spirometry. Ann Am Thorac Soc. 2018;15(12):1434-42.
4. Kinghorn B, McNamara S, Genatossio A, Sullivan E, Siegel M, Bauer I, et al. Comparison of Multiple Breath Washout and Spirometry in Children with Primary Ciliary Dyskinesia and Cystic Fibrosis and Healthy Controls. Annals of the American Thoracic Society. 2020;17(9):1085-93.
5. Gahleitner F, Thompson J, Jackson CL, Hueppe JF, Behan L, Dehlink E, et al. Lower airway clinical outcome measures for use in primary ciliary dyskinesia research: a scoping review. ERJ Open Res. 2021;7(4).
6. Stewart NJ, Smith LJ, Chan H-F, Eaden JA, Rajaram S, Swift AJ, et al. Lung MRI with hyperpolarised gases: current & future clinical perspectives. British journal of radiology. 2021;94.
7. Ng KL, Grist J, Gleeson F, Fraser E. Clinical Applications of Hyperpolarised Xenon-129 MRI. EMJ. 2024;9(4):48-61.

8. Mallallah F, Packham A, Lee E, Hind D. Is hyperpolarised gas magnetic resonance imaging a valid and reliable tool to detect lung health in cystic fibrosis patients? a cosmin systematic review. Journal of Cystic Fibrosis. 2021;20(6):906-19.
9. Marshall H, Horsley A, Taylor CJ, Smith L, Hughes D, Horn FC, et al. Detection of early subclinical lung disease in children with cystic fibrosis by lung ventilation imaging with hyperpolarised gas MRI. Thorax. 2017;72(8):760-2.
10. Smith L, Marshall H, Aldag I, Horn F, Collier G, Hughes D, et al. Longitudinal assessment of children with mild cystic fibrosis using hyperpolarized gas lung magnetic resonance imaging and lung clearance index. American Journal of Respiratory and Critical Care Medicine. 2018;197(3):397-400.
11. Smith LJ, West N, Hughes D, Marshall H, Johns CS, Stewart NJ, et al. Imaging Lung Function Abnormalities in Primary Ciliary Dyskinesia Using Hyperpolarized Gas Ventilation MRI. Annals of the American Thoracic Society. 2018;15(12):1487-90.
12. Geiger J, Zeimpekis KG, Jung A, Moeller A, Kellenberger CJ. Clinical application of ultrashort echo-time MRI for lung pathologies in children. Clinical Radiology. 2021;76(9):708.e9-.e17.
13. Hatabu H, Ohno Y, Gefter WB, Parraga G, Madore B, Lee KS, et al. Expanding Applications of Pulmonary MRI in the Clinical Evaluation of Lung Disorders: Fleischner Society Position Paper. Radiology. 2020;297(2):286-301.
14. Wucherpfennig L, Wuennemann F, Eichinger M, Schmitt N, Seitz A, Baumann I, et al. Magnetic Resonance Imaging of Pulmonary and Paranasal Sinus Abnormalities in Children with Primary Ciliary Dyskinesia Compared to Children with Cystic Fibrosis. Annals of the American Thoracic Society. 2024;21(3):438-48.
15. Montella S, Santamaria F, Salvatore M, Maglione M, Iacotucci P, De Santi MM, Mollica C. Lung disease assessment in primary ciliary dyskinesia: a comparison between chest high-field magnetic resonance imaging and high-resolution computed tomography findings. Italian Journal of Pediatrics. 2009;35(1):24.
16. Schofield L, Hind D, Singh SJ, Wild J. Study protocol: ASPECT-PCD https://figshare.com/s/c585dc4ac09edbfff7df?file=32605832: Figshare; 2021 [
17. Lucas JS, Barbato A, Collins SA, Goutaki M, Behan L, Caudri D, et al. European Respiratory Society guidelines for the diagnosis of primary ciliary dyskinesia. European Respiratory Journal. 2017;49(1).
18. Stewart NJ, Norquay G, Griffiths PD, Wild JM. Feasibility of human lung ventilation imaging using highly polarized naturally abundant xenon and optimized three-dimensional steady-state free precession. Magnetic Resonance in Medicine. 2015;74(2):346-52.
19. Norquay G, Collier GJ, Rao M, Stewart NJ, Wild JM. 129Xe-Rb Spin-Exchange Optical Pumping with High Photon Efficiency. Physical Review Letters. 2018;121(15):153201.
20. Smith LJ, Horsley A, Bray J, Hughes PJC, Biancardi A, Norquay G, et al. The assessment of short- and long-term changes in lung function in cystic fibrosis using Xe MRI. European Respiratory Journal. 2020;56(6):2000441.
21. Collier G, Acunzo L, Smith L, Hughes P, Norquay G, Chan H, et al., editors. Linear binning maps for image analysis of pulmonary ventilation with hyperpolarized gas MRI: transferability and clinical applications. Proceedings of the 26th annual meeting of ISMRM; 2018.

22. Hughes PJC, Smith L, Chan HF, Tahir BA, Norquay G, Collier GJ, et al. Assessment of the influence of lung inflation state on the quantitative parameters derived from hyperpolarized gas lung ventilation MRI in healthy volunteers. J Appl Physiol (1985). 2019;126(1):183-92.
23. Johnson KM, Fain SB, Schiebler ML, Nagle S. Optimized 3D ultrashort echo time pulmonary MRI. Magnetic Resonance in Medicine. 2013;70(5):1241-50.
24. Miller MR, Hankinson J, Brusasco V, Burgos F, Casaburi R, Coates A, et al. Standardisation of spirometry. The European respiratory journal. 2005;26(2):319-38.
25. Quanjer PH, Stanojevic S, Cole TJ, Baur X, Hall GL, Culver BH, et al. Multi-ethnic reference values for spirometry for the 3-95-yr age range: the global lung function 2012 equations. The European respiratory journal. 2012;40(6):1324-43.
26. Behan L, Leigh MW, Dell SD, Quittner AL, Hogg C, Lucas JS. Validation of pediatric health-related quality of life instruments for primary ciliary dyskinesia (QOL-PCD). Pediatr Pulmonol. 2019;54(12):2011-20.
27. Chan H-F, Smith LJ, Biancardi AM, Bray J, Marshall H, Hughes PJC, et al. Image Phenotyping of Preterm-Born Children Using Hyperpolarized ^{129}Xe Lung Magnetic Resonance Imaging and Multiple-Breath Washout. American Journal of Respiratory and Critical Care Medicine. 2023;207(1):89-100.
28. Graham BL, Steenbruggen I, Miller MR, Barjaktarevic IZ, Cooper BG, Hall GL, et al. Standardization of Spirometry 2019 Update. An Official American Thoracic Society and European Respiratory Society Technical Statement. American Journal of Respiratory and Critical Care Medicine. 2019;200(8):e70-e88.
29. Wee W, Zanette B, Munidasa S, Braganza S, Li D, Eddy R, et al. Multisite Hyperpolarized ^{129}Xe MRI Study of Pediatric Primary Ciliary Dyskinesia. European Respiratory Journal. 2023;62(67):PA3995.
30. Willmering MM, Roach DJ, Kramer EL, Walkup LL, Cleveland ZI, Woods JC. Sensitive structural and functional measurements and 1-year pulmonary outcomes in pediatric cystic fibrosis. J Cyst Fibros. 2021;20(3):533-9.
31. Thomen RP, Walkup LL, Roach DJ, Cleveland ZI, Clancy JP, Woods JC. Hyperpolarized (129)Xe for investigation of mild cystic fibrosis lung disease in pediatric patients. J Cyst Fibros. 2017;16(2):275-82.
32. de Lange EE, Altes TA, Patrie JT, Gaare JD, Knake JJ, Mugler III JP, Platts-Mills TA. Evaluation of asthma with hyperpolarized helium-3 MRI: correlation with clinical severity and spirometry. Chest. 2006;130(4):1055-62.
33. Kanhere N, Couch MJ, Kowalik K, Zanette B, Rayment JH, Manson D, et al. Correlation of Lung Clearance Index with Hyperpolarized (129)Xe Magnetic Resonance Imaging in Pediatric Subjects with Cystic Fibrosis. Am J Respir Crit Care Med. 2017;196(8):1073-5.
34. Couch MJ, Munidasa S, Rayment JH, Voskrebenzev A, Seethamraju RT, Vogel-Claussen J, et al. Comparison of Functional Free-Breathing Pulmonary (1)H and Hyperpolarized (129)Xe Magnetic Resonance Imaging in Pediatric Cystic Fibrosis. Acad Radiol. 2021;28(8):e209-e18.
35. Kinghorn B, Rosenfeld M, Sullivan E, Onchiri F, Ferkol TW, Sagel SD, et al. Airway Disease in Children with Primary Ciliary Dyskinesia: Impact of Ciliary Ultrastructure Defect and Genotype. Annals of the American Thoracic Society. 2023;20(4):539-47.
36. Magnin ML, Cros P, Beydon N, Mahloul M, Tamalet A, Escudier E, et al. Longitudinal lung function and structural changes in children with primary ciliary dyskinesia. Pediatr Pulmonol. 2012;47(8):816-25.

37. Tadd K, Morgan L, Rosenow T, Schultz A, Susanto C, Murray C, Robinson P. CF derived scoring systems do not fully describe the range of structural changes seen on CT scans in PCD. Pediatric Pulmonology. 2019;54(4):471-7.
38. Jain K, Padley S, Goldstraw E, Kidd S, Hogg C, Biggart E, Bush A. Primary ciliary dyskinesia in the paediatric population: range and severity of radiological findings in a cohort of patients receiving tertiary care. Clinical radiology. 2007;62(10):986-93.

*Table 1: Participant demographics including ultrastructural defects. Data is presented as mean ± SD or median (IQR) depending on if data is normally distributed. Ultrastructural defects within study population presented as n= (%). IDA=inner dynein arm defect, ODA= outer dynein arm defect, MTD= microtubular disarrangement. *PCD diagnosis confirmed by genetics. PsA=Pseudomonas aeruginosa.*

Clinical data (n=35)	**Data reported as n (%), mean ± SD, or median (IQR)**
Sex	19 male (54%)
Age (years)	12.3 ± 3.3
Age at diagnosis (years)	3 (0, 6)
Ultrastructural defect	
IDA or MTD only	9 (25.7%)
ODA only	8 (22.9%)
IDA and ODA	12 (34.3%)
No defect*	6 (17.1%)
Situs inversus	14 (40.0%)
No. of antibiotic courses in last 12 months (oral or IV, planned or unplanned)	2.5 (1,4)
PsA (cultured in last 12 months)	5 (14.3%)

Table 2: Spirometry and ^{129}Xe MRI metrics

	Data reported as mean ±SD or median (IQR)	
Spirometry (n=34)	z-score	% predicted
FEV_1	-1.5 ± 1.7	81.3 ± 20.6
FVC	-0.7 ± 1.5	90.1 ± 21.6
FEV_1/FVC	-1.5 ± 1.3	87.2 ± 11.7
^{129}Xe MRI (n=35)		
VDP (%)	6.3 (1.3,16.1)	
VHI (%)	11.3 ± 3.2	

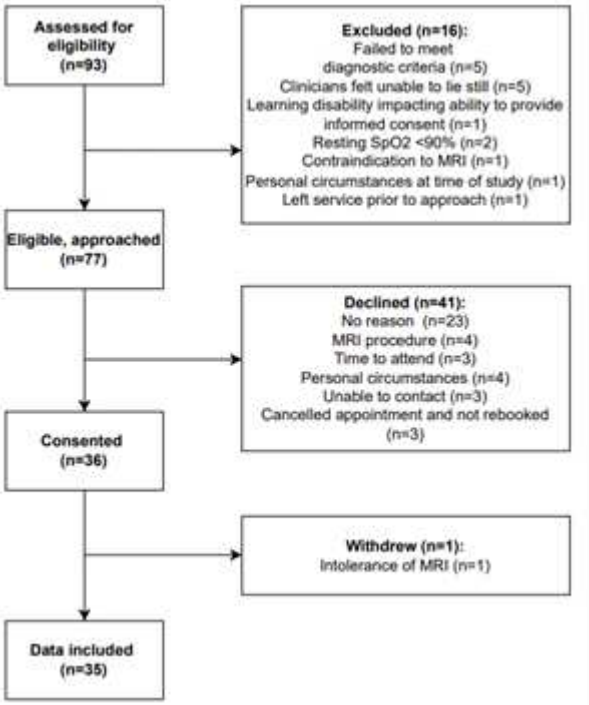

Figure 1

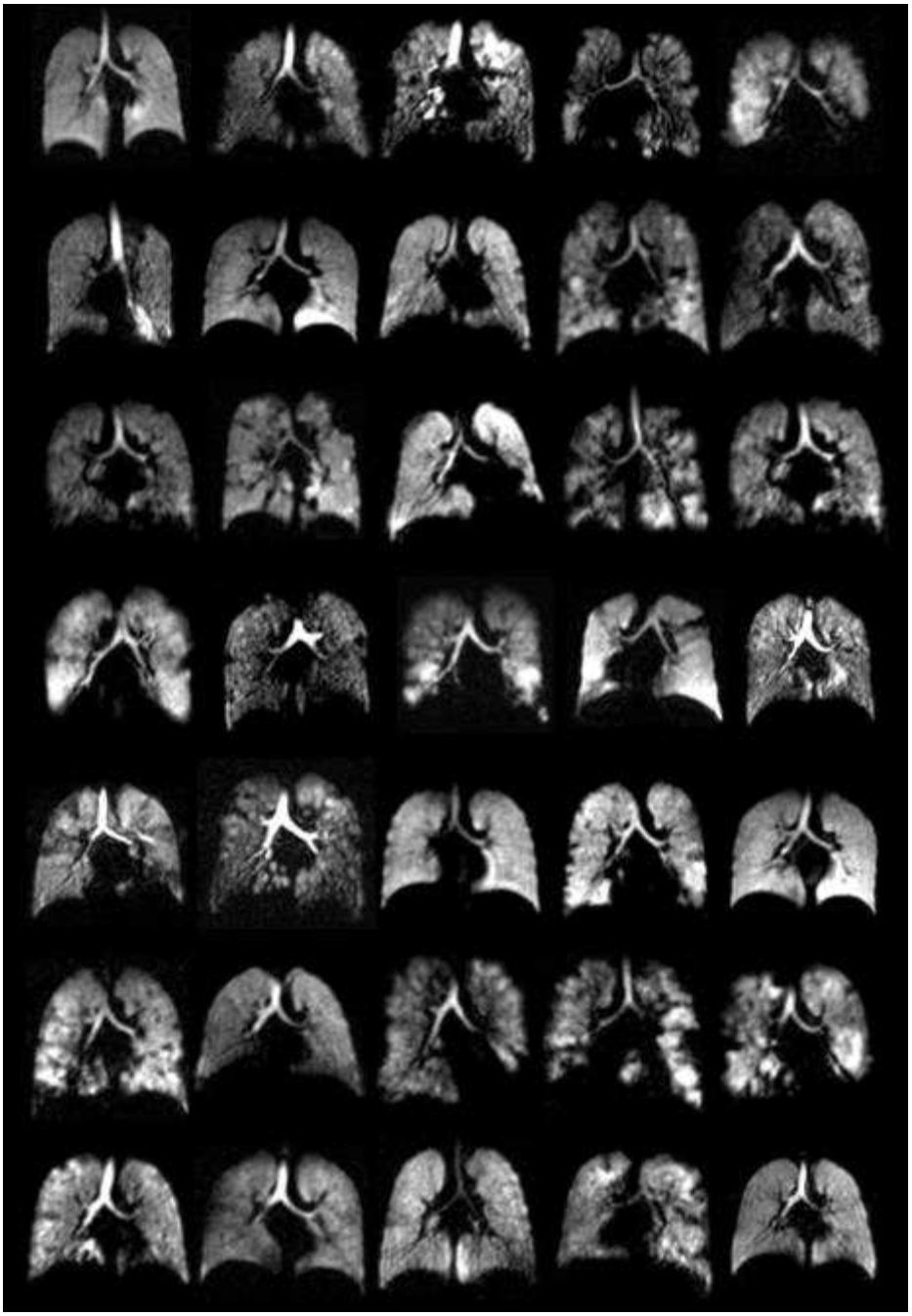

Figure 2

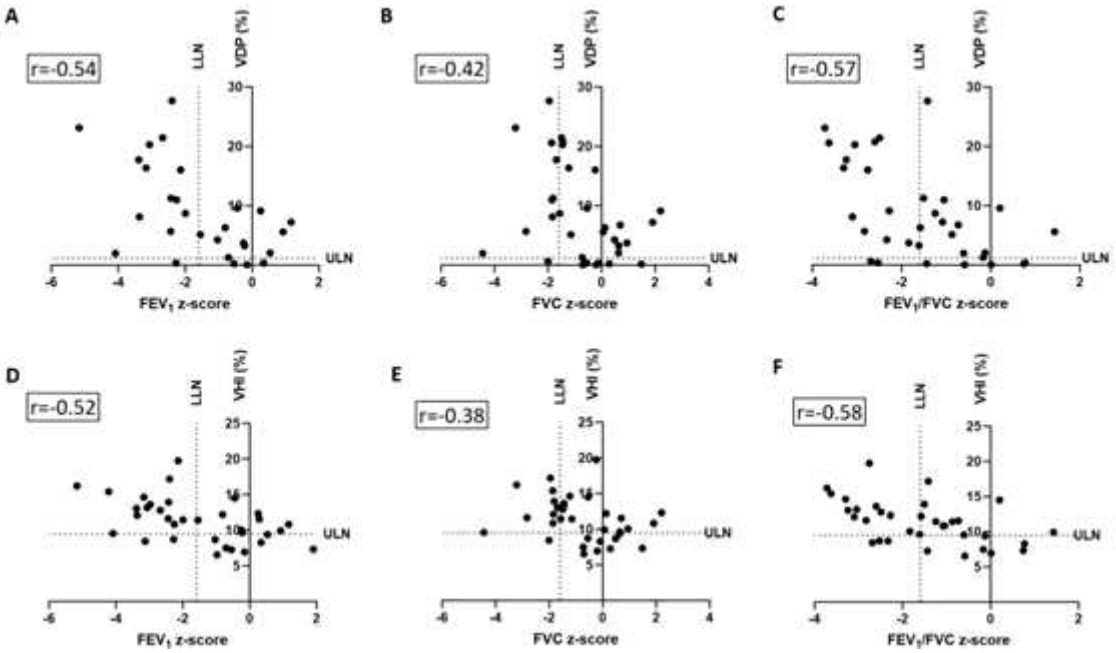

Figure 3

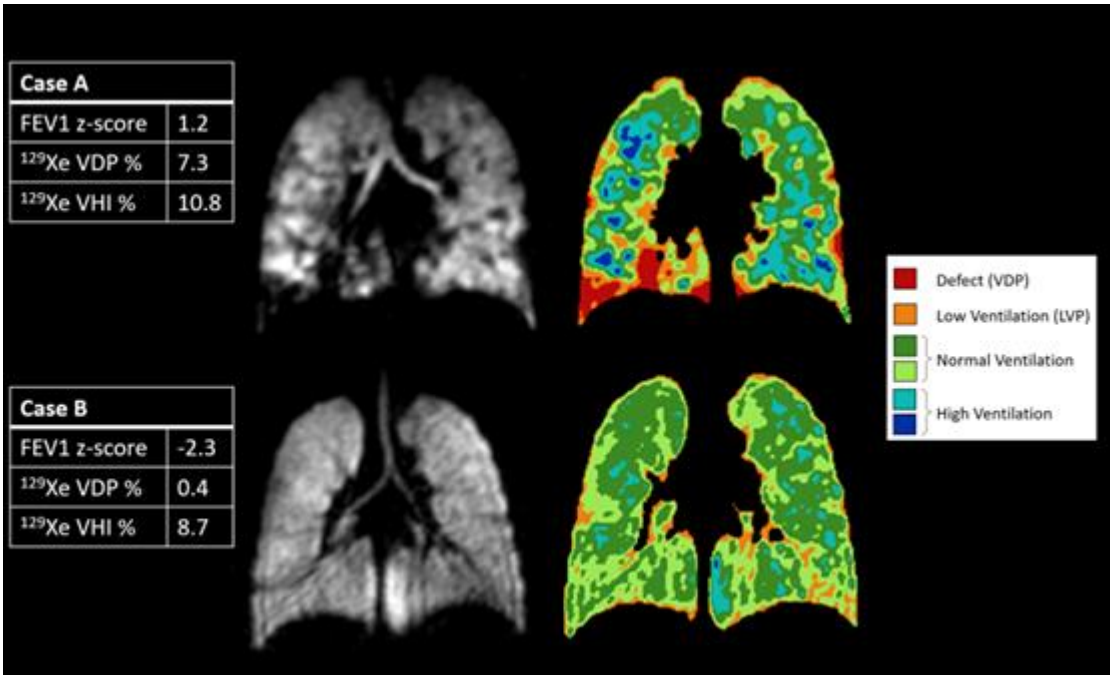

Figure 4

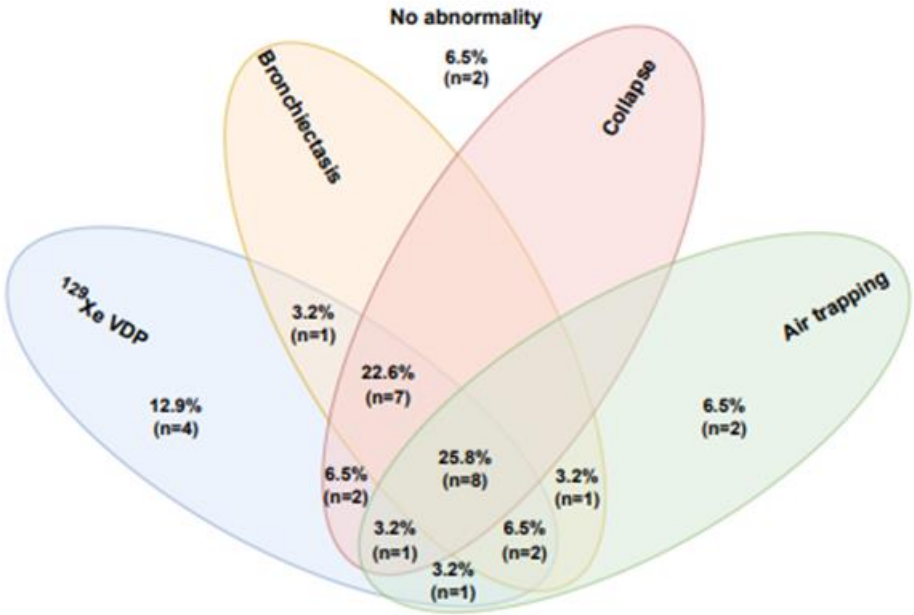

Figure 5

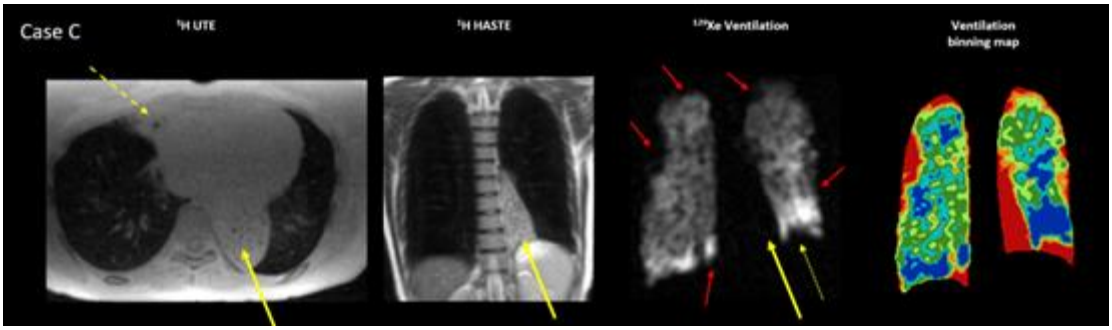

Figure 6

Image acquisition

Details of the imaging sequences are provided in Table S1.

Table S1: Overview of imaging sequences performed.

3D Spoiled Gradient Echo (SPGR)  **Description:** T1 weighted images, taken at an end inspiratory tidal volume (EITV). **Role:** Images used for VDP calculation. **Scan details:** Plane: Coronal. Slice thickness 5.0mm, 36 slices per acquisition. Field of view (FOV) 40.0cm. Scan duration: Typically, 6 second breath hold at EITV. Coil: body transmit-receive coil.
Hyperpolarised ^{129}Xe gas ventilation steady state free precision  **Description:** Imaging of lung ventilation with ^{129}Xe as contrast. **Role:** Functional MRI scan. Signal from ^{129}Xe offers visualisation of the distribution of ventilation. Used to calculate metrics and for visual analysis of ventilation. **Metrics:** ^{129}Xe VDP and VHI. **Scan details:** Steady state free precession sequence. Plane: Coronal. Slice thickness: 10.0mm FOV 40.0cm. Scan duration: Typically, 6 second breath hold at EITV. Coil: ^{129}Xe transmit receive flex quad coil
Ultra-short echo (UTE)  **Description:** Proton density weighted sequence which provides high-resolution isotropic 3D images. **Role:** Structural MRI scan. Visualisation of the lung parenchyma with high-resolution, similar in contrast to CT. **Scan details:** Plane: Any (isotropic). resolution 1.3 mm isotropic. FOV 35cm. Scan duration: 8 to 9 minutes, relaxed breathing, data prospectively or retrospectively gated to expiration (i.e. at a lung volume near FRC). Coil: 8 channel array (HDxt) or 16+ channel anterior array + spine array.
Steady State Free Precession (SSFP)  **Description:** Offers a combination of T1 and T2 weighted contrast with hyper intense signal from long T2 components. **Role:** Structural MRI scan. Allows visualisation of anatomy and can visualise mucus. **Scan details:** Plane: Axial, 25 slices Slice thickness: 10mm. FOV 40.0cm. Scan duration: Typically, 8 second expiratory breath hold. Coil: 8 channel array.
Half-Fourier-Acquired Single-shot Turbo Spin Echo (HASTE)  **Description:** A rapid T2 weighted sequence. **Role:** Structural MRI scan. Allows visualisation of mucus. The acquisition speed reduces the impact of motion on the images. **Scan details:** Plane: Coronal. Slice thickness: 10mm, 18 slices. FOV 35.0cm. Scan duration: Typically, 8 second inspiratory breath-hold. Coil: 8 channel array
3D Spoiled Gradient Echo (SPGR) with isotropic voxel size

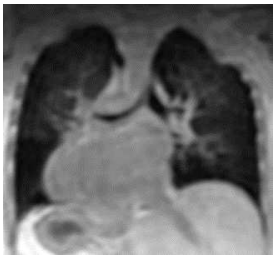

Description: T1 weighted images (as above), taken at EITV and approximately RV.
Role: At higher lung volumes images may visualise mucus, and at lower volumes air trapping.
Scan details: Plane: Any (isotropic) Slice thickness 3.0mm, 62 slices per acquisition. FOV 40.0cm. Scan duration: Typically, 6 second breath hold at TLC, EITV and RV. Coil: 8 channel array

^{129}Xe MRI image acquisition

Hyperpolarised gas ventilation images were acquired by inhaling a titrated mixture of ^{129}Xe and medical grade nitrogen, which were administered via a Tedlar plastic bag. An MRI scanner sequence which only images the ^{129}Xe gas is used in combination with a dedicated ^{129}Xe coil, to image the areas of the lung which have been ventilated by the polarised gas. Images were acquired during a single breath-hold, taken at an estimated end-inspiratory tidal volume (EITV). Participants were coached to perform at least two relaxed tidal breaths before then inhaling a fixed volume of the gas from a resting FRC lung volume. The total volume of inhaled gas was calculated based on the participant's height with the aim of achieving an approximate same lung inflation level across the group irrespective of the participant's size. This process of inhaling the volume of the bag from FRC provided an estimated volume of 60% of TLC, referred to as EITV. The volume of the gas, which ranged from 0.4 to 1.0 L comprised a scaled dose of ^{129}Xe balanced with medical grade Nitrogen as shown in Table S2, in line with previously published methods (1).

Table S2: Inhaled gas volume and composition height-based calculations.

Patient height (standing)	Total volume	Gas mixture composition
Over 160cm	1.0 L	500 ml ^{129}Xe + 500 ml N_2
150-160cm	800 ml	450 ml ^{129}Xe + 350 ml N_2
140-150cm	650 ml	400 ml ^{129}Xe + 250 ml N_2
130-140cm	500 ml	350 ml ^{129}Xe + 150 ml N_2
Less than 130cm	400 ml	300 ml ^{129}Xe + 100 ml N_2

Calculation of VDP and VHI

^{1}H matched anatomical images were registered to the ^{129}Xe ventilation images. Segmentation of the registered anatomical images was completed using in house software via MATLAB (MathWorks, Natick, MA) with a semi-automated process. An initial automated map of the estimated lung cavity was generated using deep-learning (2) or a combined approach employing deep-learning and fuzzy-c means clustering (3-5) which was then corrected as needed by manual editing to give the thoracic cavity volume (TCV). For individuals with situs inversus, images were flipped on a vertical axis prior to segmentation to optimise performance of the automated deep-learning segmentation. Images were flipped back to situs inversus orientation after the segmentation was completed. The ^{129}Xe ventilation signal was categorised using an automated linear "binning" process (6) in which voxels were sorted from low to high signal, to form a linear distribution and the signal was divided by the mean ventilation signal within the thoracic cavity. This ventilation distribution was then divided into six categories known as "bins" centred around the mean signal and with the width of each bin equal to one standard deviation. The two central bins were combined into a single normal ventilation bin, the two highest signal bins combined into a single high ventilation bin. Each voxel was therefore assigned into one of four bins: high ventilation, normal ventilation, low ventilation, or ventilation defect. ^{129}Xe VDP, the proportion of the lung with no ventilation, was calculated as the ventilation defect volume from bin 1 / TCV * 100. ^{129}Xe VHI was calculated using an in-house automated process which assesses each ventilated voxel with the eight in-plane adjacent voxels using an established method (7). From this, a map of the co-efficient of variation of signal intensity is produced and the interquartile range of the coefficient of variation of signal intensity is used as the ventilation heterogeneity index (VHI).

TableS3: MRI scan sequence order with details of coil used.

Order	Image sequence	Coil
1	^{129}Xe at EITV	^{129}Xe transmit-receive vest
2	SPGR at EITV	In-built transmit receive
3	HASTE	^{1}H array
4	SPGR at EITV	
5	SPGR at RV	
6	SSFP	
7	UTE	

Table S4: Study visit schedule.

Order and content of study visit
1 Height and weight
2 Spirometry
3 Oxygen saturations (finger probe)
4 Pre-ACT MRI (0 hours)
5 ACT completion
6 MRI (+2 hours from baseline)
7 QOL-PCD
8 MRI (+6 hours from baseline)

Table S5: QOL-PCD scores

QOL-PCD	**Data reported as mean ±SD or median (IQR)**		
Domain	Child (n=17)	Adolescent (n=16)	Parent proxy (n=16)
Physical functioning	69.4 ± 21.0%	80.6 ± 26.5%	71.3 ± 26.8%
Emotional functioning	69.6 ± 16.7%	80.2% ± 16.9%	67.4 ± 18.8%
Treatment burden	62.3 ± 27.1%	72.2 ± 23.3%	63.0 ± 19.2%
Role	N/A	78.4 ± 20.8%	N/A
Social functioning	71.0 ± 30.2%	70.8 ± 19.3 %	75.7 ± 17.3%
Vitality	N/A	59.7 ± 27.8%	N/A
Upper respiratory symptoms	63.1 ± 26.7%	74.2 ± 15.6%	47.9 ± 18.4%
Lower respiratory symptoms	58.0 ± 22.9%	75.6 ± 15.8%	55.4 ± 19.7%
Hearing	69.6 ± 26.2%	93.2 ± 9.2%	77.8 ± 21.8%
Eating and weight	N/A	N/A	76.2 ± 27.8%
Health perception	N/A	N/A	67.0 ± 16.9%

Table S6: Diagnostic information for participants taken from clinical data: cilial ultrastructural abnormalities, genetic defects and nasal nitric oxide in ppb (parts per billion).

No	Ultrastructural abnormality	Genetic defect	Nasal nitric oxide (ppb)
1	IDA	Nil on record	29
2	Normal	DNAH11	213
3	ODA	DNAH5	Nil on record
4	IDA	CCDC39	14
5	IDA	HYDIN	<5
6	IDA+ODA	DNAH5	49

7	IDA+ODA	SPAG1	20
8	IDA+ODA	DNAH5	42
9	ODA	DNAH5	24
10	IDA+ODA	DNAH5	20
11	IDA+ODA	DNAAF5	<5
12	IDA+ODA	Nil on record	19
13	IDA+ODA	DNAH5	9
14	MTD	CCDC40	12
15	IDA+ODA	DNAAf5	5
16	IDA+ODA	CCDC103	49
17	Normal	CCDC103	537
18	IDA	Nil identified	51
19	Normal	LRRCG	680
20	MTD	Nil identified	30
21	ODA	DNAH5	67
22	MTD	RSPH4A	91
23	Normal	DNAH11	307
24	IDA + ODA	CCDC40	32
25	IDA	DNAH5	39
26	ODA	DNAH11	40
27	Normal	DRC1	116
28	IDA+ODA	LRRC6	<5
29	IDA+ODA	CCDC40	23
30	ODA	Nil on record	<5
31	ODA	DNAH5	18
32	Normal	DNAH11	30
33	ODA	Nil identified	355
34	IDA+ODA	DNAH5	22
35	ODA	DRC1	551

References

1. Smith LJ, Horsley A, Bray J, et al. The assessment of short- and long-term changes in lung function in cystic fibrosis using Xe MRI. European Respiratory Journal. 2020;56(6):2000441.
2. Astley JR, Biancardi AM, Marshall H, et al. A Dual-Channel Deep Learning Approach for Lung Cavity Estimation From Hyperpolarized Gas and Proton MRI. Journal of Magnetic Resonance Imaging. 2023;57(6):1878-90.
3. Bertin FJ, Collier GJ, Hughes PJ, et al. Simultaneous segmentation of airways and ventilated lung in hyperpolarised-gas MR images by deep learning. International Society for Magnetic Resonance in Medicine. 2021;3226.
4. Bertin F, Collier G, Hughes P, et al., editors. A Deep-Learning Approach to Hyperpolarised-Gas MR Image Segmentation. BioMedEng 2021; 2021; Sheffield: BioMedEng Association.
5. Biancardi A, Acunzo L, Marshall H, et al., editors. A paired approach to the segmentation of proton and hyperpolarized gas MR images of the lungs. Proceedings of the 26th Annual Meeting of ISMRM Volume (abstract 2442); 2018: ISMRM Paris.
6. Collier G, Acunzo L, Smith L, et al., editors. Linear binning maps for image analysis of pulmonary ventilation with hyperpolarized gas MRI: transferability and clinical applications. Proceedings of the 26th annual meeting of ISMRM; 2018.
7. Hughes PJC, Smith L, Chan HF, et al. Assessment of the influence of lung inflation state on the quantitative parameters derived from hyperpolarized gas lung ventilation MRI in healthy volunteers. J Appl Physiol (1985). 2019;126(1):183-92.